⌘ *Author's Choice*

THE JOURNAL OF BIOLOGICAL CHEMISTRY VOL. 287, NO. 27, pp. 22927–22937, June 29, 2012

Anti-carcinoembryonic Antigen Single-chain Variable Fragment Antibody Variants Bind Mouse and Human Neonatal Fc Receptor with Different Affinities That Reveal Distinct Cross-species Differences in Serum Half-life*[S]

Received for publication, February 24, 2012, and in revised form, April 27, 2012 Published, JBC Papers in Press, May 8, 2012, DOI 10.1074/jbc.M112.355131

Jan Terje Andersen[‡§1], Stian Foss[‡§], Vania E. Kenanova[¶2], Tove Olafsen[¶3], Ingvild S. Leikfoss[‡§‖4], Derry C. Roopenian[**], Anna M. Wu[¶], and Inger Sandlie[‡§5]

*From the [‡]Centre for Immune Regulation and Department of Molecular Biosciences, University of Oslo, N-0316 Oslo, Norway, the [§]Centre for Immune Regulation and Department of Immunology, Rikshospitalet University Hospital, N-0424 Oslo, Norway, the [¶]Crump Institute for Molecular Imaging, Department of Molecular and Medical Pharmacology, David Geffen School of Medicine at UCLA, Los Angeles, California 90095, the [‖]Institute of Basic Medical Sciences, University of Oslo, P. O. Box 1105 Blindern, N-0317 Oslo, Norway, and **The Jackson Laboratory, Bar Harbor, Maine 04609*

Background: FcRn regulates the serum half-life of IgG.
Results: Fc engineering of scFv-Fc affects binding to mFcRn and hFcRn differently, which reflects blood clearance in WT and transgenic mice.
Conclusion: Modulating FcRn binding to scFv-Fc reveals cross-species differences that determine blood clearance.
Significance: This work provides insights into FcRn binding that must be considered prior to pre-clinical evaluation of engineered IgGs.

Serum half-life of IgG is controlled by the neonatal Fc receptor (FcRn) that interacts with the IgG Fc region and may be increased or decreased as a function of altered FcRn binding. Preclinical evaluations of modified IgGs are frequently carried out in mice, but such IgGs may bind differently to mouse and human FcRn (mFcRn and hFcRn). Here, we report a detailed characterization of a matched set of mouse-human chimeric T84.66 scFv-Fc variants with specificity for the tumor carcinoembryonic antigen and mutations in the FcRn-binding site. Binding to soluble mFcRn and hFcRn was measured using *in vitro* assays, and the results were compared with blood clearance *in vivo* in normal (mFcRn bearing) and hFcRn transgenic mice. All variants bound better to mFcRn than to hFcRn. The loss of affinity varied among the mutants, however, and also the hierarchy of binding differed depending on the receptor. The mutations had no major impact on binding to the classical Fcγ receptors. Importantly, the trend of blood clearance in both strains of mice correlated with the hierarchy of binding obtained using soluble FcRn. Consequently, *in vitro* interaction analysis of engineered IgGs regarding their cross-species FcRn binding ability provides information for prediction of *in vivo* pharmacokinetics.

Monoclonal antibodies and their modified recombinant fragments conjugated to radioisotopes and toxic drugs, termed immunoconjugates, are of clinical value in anti-tumor imaging and therapy. The utility of these immunoconjugates, when administered *in vivo*, depends on their pharmacokinetics and biodistribution. The main challenge is to balance retention at the target site with the rate as well as site of clearance to maximize efficacy while avoiding toxicity to kidneys, liver, bone marrow, or other normal tissues. Different radionuclides and several antibody formats with a spectrum of *in vivo* properties for a given application have been reported (1–3).

The long and relatively constant serum half-life of intact IgG (~22 days) and recombinant Fc-conjugated drugs is regulated by the major histocompatibility class I-related FcRn[6] (4–6). This receptor is localized in a wide range of cell types and tissues, including vital organs such as the kidneys (7) and the liver (8, 9) as well as circulating immune cells (10–12) and vascular endothelial cells lining the blood circulation (13, 14). Thus, the global presence of FcRn has a great impact on biodistribution of IgG molecules throughout the body.

* This work was supported, in whole or in part, by National Institutes of Health Grants CA043902, CA086306, and CA016042 (to V. E. K., T. O., and A. M. W.).
⌘ *Author's Choice*—Final version full access.
[S] This article contains supplemental Tables 1–3 and Figs. 1–4.
[1] Supported by Norwegian Research Council Grant 179573/V40 and South-Eastern Norway Regional Health Authority Grant 9375. To whom correspondence may be addressed: Centre for Immune Regulation and Dept. of Immunology, Oslo University Hospital Rikshospitalet and University of Oslo, P. O. Box 4956, Oslo N-0424, Norway. E-mail: j.t.andersen@imbv.uio.no.
[2] Present address: Novartis Institute for Biomedical Research Inc., Cambridge, MA 02139.
[3] Present address: ImaginAb, Inc., 440 Hindry Ave., Suite E, Inglewood, CA 90301.
[4] Present address: Dept. of Neurology, Oslo University Hospital, Oslo, P. O. Box 1105 Nydalen, N0407, Norway.
[5] To whom correspondence may be addressed: Centre for Immune Regulation (CIR) and Dept. of Immunology, Oslo University Hospital Rikshospitalet and University of Oslo, PO Box 4956, Oslo N-0424, Norway. E-mail: inger.sandlie@imbv.uio.no.

[6] The abbreviations used are: FcRn, neonatal Fc receptor; CEA, carcinoembryonic antigen; HC, heavy chain; HER2, human epidermal growth factor receptor 2; hFcRn, human FcRn; mFcRn, mouse FcRn; FcγRs, Fcγ receptor; SPR, surface plasmon resonance; RU, resonance unit; Req, responses obtained at equilibrium.

The fundamental importance of FcRn in IgG homeostasis has been demonstrated using an engineered mouse strain in which FcRn can be conditionally deleted in both endothelial and hematopoietic cells. Lack of FcRn expression in these cells resulted in a 4-fold lower serum level of IgG than what was found in wild type (WT) mice, whereas the half-life of an exogenous injected human IgG1 (hIgG1) decreased by 21-fold (13).

The cellular mechanism by which IgGs are rescued has been revealed using advanced microscopy technologies (15, 16), where IgG, continually taken up by fluid phase endocytosis, is delivered to early endosomes, where FcRn predominantly resides. The acidified endosomal environment favors pH-dependent binding of the Fc part of IgG to FcRn. After binding, the complex is recycled to the cell surface, where the physiological pH of the blood triggers release of IgG. Thus, IgG Fc containing molecules are rescued from lysosomal degradation via an efficient FcRn-mediated recycling pathway.

The interaction site for FcRn on IgG (human and rodents) has been mapped using site-directed mutagenesis as well as x-ray crystallography and shown to involve negatively charged residues on the α2-domain of the FcRn heavy chain (HC) (Glu-115 and Glu-116) and conserved amino acid residues localized to the C_H2-C_H3 IgG Fc interface that include three highly conserved key residues, namely Ile-253, His-310, and His-435 (17–19). The central role of the histidine residues reflects the strictly pH-dependent mode of binding that is explained by the imidazole side chain that is neutral at physiological pH and positively charged at acidic pH.

Despite conservation of the key residues across species, hFcRn discriminates between IgG from several species, including mouse IgGs (mIgG), that do not interact, except from weak binding of mIgG2b (20–22). This fact largely explains the disappointing results obtained from clinical trials during the 1980s using murine monoclonal IgGs and also why mouse immunoconjugates, such as ^{131}I-tositumomab (Bexxar, Cortixa Corp.) and ^{90}Y-ibritumomab-tiuxetan (Zevalin, IDEC Pharmaceuticals Corp.), are cleared very rapidly from the circulation.

Engineered hIgG1 and hIgG2 with improved affinity for hFcRn at acidic pH show increased serum half-lives in primates (21, 23, 24). However, negligible binding at physiological pH is necessary (4, 23–26), and an increase has the opposite effect. This has been exemplified for a new class of engineered antibodies, termed Abdegs (enhancing IgG degradation), with short serum half-life that furthermore accelerates the clearance of circulating IgGs due to saturation of binding to FcRn that blocks further IgG binding (27, 28). However, favorable binding to hFcRn does not necessarily imply similar binding kinetics toward mFcRn, as for instance demonstrated by the hIgG1 variant with two Fc point mutations (H433K/N434F) that results in a 4-fold reduced serum half-life in WT mice but enhanced transport in an *ex vivo* human placenta model system (29).

One may alter the half-life of immunoconjugates by reducing the size or by introducing site-directed mutations, as exemplified by antibody derivatives with specificity for the tumor antigen carcinoembryonic antigen (CEA) (30–33). CEA is found in colorectal, breast, and lung cancers but also in low amounts in noncancerous tissue. The concentration of the antigen in tumors is ~60 times higher than that in healthy tissue (34, 35), and thus, CEA is an attractive candidate for antibody-based tumor targeting in diagnostic imaging and radioimmunotherapy.

Several different recombinant anti-CEA T84.66 antibody derivatives have been generated, and their *in vivo* tumor targeting properties and biodistribution were investigated in mice (3). For instance, the minibody (scFv-C_H3) format demonstrates fast clearance, excellent tumor uptake, and high contrast images in both LS174T xenografted mice and in a clinical pilot study (30–33). A set of anti-CEA T84.66 chimeric mouse-human scFv-Fc mutants showed a spectrum of *in vivo* half-lives and positron emission tomography imaging properties in BALB/c mice and tumor-bearing LS174T xenografted athymic mice (36, 37). Five scFv-Fc mutants were produced, termed I253A, H310A, H435Q, H435R, and H310A/H435Q (EU numbering system).

In this study, we thoroughly investigate the cross-species binding properties of these scFv-Fc variants toward the mouse and human forms of FcRn and the classical FcγRs using enzyme-linked immunosorbent assays (ELISA) and surface plasmon resonance (SPR) measurements. Furthermore, we measure the serum half-life in mice transgenic for hFcRn.

We find that the interaction properties of the scFv-Fc variants toward mFcRn correlated well with the *in vivo* serum half-lives and tissue biodistribution obtained in WT mice. Interestingly, binding to hFcRn was distinct from that of mFcRn and correlated with serum half-lives obtained from *in vivo* clearance studies performed in mice transgenic for hFcRn. In such mice, the half-life values were considerably shorter than those obtained in WT mice, and the clearance rate hierarchy among the variants was changed. Such variations in FcRn binding across species as well as differences in half-life obtained using different preclinical models must be taken into account prior to predicting pharmacokinetics in humans.

EXPERIMENTAL PROCEDURES

Construction, Production, and Purification of anti-CEA scFv-Fc Antibody Fragments—The anti-CEA cT84.66 scFv-Fc WT (nonmutated) and mutants (H435Q, H435R, H310A, I253A, and H310A/H435Q) used in these studies have been previously described (36, 37). The scFv-Fc proteins were expressed in NS0 murine myeloma cells following transfection of the mammalian expression vector pEE12 containing the scFv-Fc cDNAs, driven by the human cytomegalovirus promoter and a glutamine synthetase selection marker. Collected supernatants were centrifuged to remove cell debris and treated with AG1-X8 resin (Bio-Rad) in phosphate buffered saline (PBS) to remove phenol red. Then the fractions were filtrated and dialyzed against 50 mM Tris-HCl (pH 7.4). Recombinant scFv-Fc variants were purified using protein A affinity chromatography (Poros 20A, Applied Biosystems) using the GE Pharmacia AKTA purifier FPLC system (GE Healthcare), where PBS was used to equilibrate the column prior to loading the sample. Bound protein was eluted with a linear pH gradient (pH 7.0 to pH 2.1) using 0.2 M citrate buffer. Eluted protein was immediately neutralized with 80% v/v of 1 M Tris-HCl (pH 8.2), pooled, and dialyzed in 1× PBS. Then anion exchange chromatography using a Source HQ50 column (Amersham Biosciences) fol-

lowed by a ceramic hydroxyapatite column (Bio-Rad) and anion exchange chromatography using a Source 15Q column (Amersham Biosciences) were performed, all as described previously (36). The final fractions were pooled, dialyzed against PBS, and concentrated by Centriprep 30 (Millipore Corp., Bedford, MA). Absorbance was monitored at 280 nm, and final protein concentration was determined using a NanoDrop 2000 spectrophotometer (Thermo Fisher Scientific). The A_{280} value was divided by an extinction coefficient of 1.4.

Construction, Production, and Purification of Recombinant Soluble Forms of Mouse and Human Fcγ Receptors and FcRn Variants—Vectors containing truncated versions of mFcRn and hFcRn HC cDNAs encoding their three ectodomains (α1–α3) genetically fused to a cDNA encoding the *Schistosoma japonicum* glutathione *S*-transferase (GST) have been described (22, 38). The vectors denoted pcDNA3-hFcRn-GST-hβ2m-oriP and pcDNA3-mFcRn-GST-hβ2m-oriP also contain a cDNA encoding human β_2-microglobulin and the Epstein-Barr virus origin of replication (oriP). Soluble versions of FcRn (mFcRn and hFcRn) were produced in HEK 293E cells, and secreted receptors were purified using a GSTrap column as described (25). An mFcRn variant expressed in infected High-Five cells was a generous gift from Dr. Sally Ward (University of Texas Southwestern Medical Center, Dallas) (39).

Recombinant soluble forms consisting of the ectodomains of hFcγRI, hFcγRIIa, and hFcγRIIb, fused to GST, were produced from pcDNA3-GST-oriP vectors as described previously (40). Truncated cDNA segments encoding the extracellular domains of the human forms of FcγRIIIa and FcγRIIIb as well as the mouse forms of FcγRI FcγRIIb, FcγRIV, and FcγRIII were synthesized by Genscript and subcloned into the pcDNA3-GST-oriP using the restriction sites XhoI and HindIII and subsequently produced in HEK 293E cells as above.

ELISA—A 96-well plate (Nunc) was coated with 100 μl of recombinant CEA (0.5 μg/ml; Abcam) and incubated overnight at 4 °C followed by washing three times with 1× PBS/Tween (pH 7.4). The wells were blocked with 4% skimmed milk (Neogen Europe Ltd.) for 1 h at room temperature (RT) and washed in PBS/Tween (pH 6.0). The anti-CEA T84.66 scFv-Fc variants were diluted in 4% skimmed milk, 1× PBS/Tween (pH 6.0) as serial concentrations and added to the wells. After incubation for 1 h at RT, purified hFcRn-GST or mFcRn-GST (1 μg/ml) was diluted in 4% skimmed milk, 1× PBS/Tween (pH 6.0) and preincubated with goat HRP-conjugated anti-GST IgG (GE Healthcare) diluted 1:5000 and added to the wells. The plates were incubated for 1 h at RT and washed with 1× PBS/Tween (pH 6.0). Bound receptor was detected by adding 100 μl of the substrate 2,2′-azino-bis(3-ethylbenzothiazoline-6-sulfonic acid/H_2O_2 (Sigma) or 3,3′,5,5′-tetramethylbenzidine substrate (Calbiochem). The absorbance was measured at 405 or 450 nm using a Sunrise TECAN spectrophotometer. The assay described above was also performed using 1× PBS/Tween (pH 7.4) in all steps. In addition, the same setup was used with GST-fused versions of hFcγRI, hFcγRIIa, hFcγRIIb, hFcγRIIIa, hFcγRIIIb, mFcγRI, mFcγRIIb, mFcγRIV, and mFcγRIII. All receptors were added at 1 μg/ml except from the FcγRI variants that were added at 0.50 μg/ml. Receptor binding was visualized using a goat HRP-conjugated anti-GST antibody.

Dialysis of IgG and scFv-Fc Preparations—Prior to all SPR binding analyses, IgG variants and scFv-Fc fragments were extensively dialyzed overnight using Slide-A-Lyzer Dialysis Cassettes (cutoff at 10 kDa; 0.5-ml capacity; Pierce) at 4 °C to the same buffer used as running buffer (67 mM phosphate buffer) during the experiments. Anti-hydroxy-5-iodo-3-nitrophenylacetyl mouse IgG1 (mIgG1) was a gift from Dr. Gregory Winter (Centre for Protein Engineering, Medical Research Council Centre, UK).

Surface Plasmon Resonance—SPR experiments were carried out using a semiautomatic Biacore 3000 instrument (GE Healthcare). Flow cells of research grade CM5 sensor chips were directly coupled with GST-tagged hFcRn or mFcRn using amine coupling chemistry as described in the standard amine coupling kit (GE Healthcare). For coupling, the proteins were injected at a concentration of 10 to 1 μg/ml in 10 mM sodium acetate (pH 5.0), with contact times of 5 min at a flow rate of 5 μl/min. The approximate amounts of immobilized receptors are indicated in each experiment in resonance units (RU). Reference flow cells were prepared in an analogous manner with buffer only during the coupling cycle followed by deactivation of the dextran surface with 1 M ethanolamine. Several experiments were run with different analyte concentrations (0.0004–2 μM) of the T84.66 anti-CEA H435R, H435Q, H310A, I253A, H310A/H435Q, nonmutated WT scFv-Fc, intact T84.66 IgG1, or anti-hydroxy-5-iodo-3-nitrophenylacetyl mIgG1 over hFcRn-GST as above. All experiments were performed with 67 mM phosphate buffer containing 0.05% Tween 20 (pH 6.0 or 7.4), both as running and dilution buffers at a flow rate of 50 μl/ml at 25 °C. The running buffer at pH 7.4 was used to regenerate the flow cells at the end of each dissociation phase. To correct for nonspecific binding and bulk buffer effects, the responses obtained from the control surfaces and blank injections were subtracted from each interaction curve. Affinity constants were calculated from the resulting sensorgrams using the heterogeneous ligand binding model provided by the BIAevaluation 4.1 software. The model assumes that there are two noninteracting ligand-binding sites on the immobilized ligand.

Radioiodination—Purified scFv-Fc fragments were each radioiodinated with carrier-free ^{123}I (sodium iodide in 0.1 N NaOH from MDS Nordion) using the IODO-GEN method. Briefly, reaction volumes of 0.1 ml containing 150 μg of protein (414–520 μCi) of ^{123}I and carrier iodide at a ratio of 0.5 per antibody molecule in Pierce pre-coated iodination tubes (Thermo Fisher Scientific) were incubated for 10 min at RT. The labeling reactions were stopped by transferring the reaction mixtures into 1.6-ml microcentrifuge tubes. Labeling efficiencies were measured by instant thin layer chromatography using the monoclonal antibody instant TLC strips from Biodex Medical Systems and 0.9% NaCl as running buffer, as described (41).

Pharmacokinetic Studies in hFcRn Transgenic Mice—All animal studies were conducted under protocols approved by the Chancellor's Animal Research Committee at UCLA. Twenty four 15–16-week-old transgenic mice with a homozygous mFcRn gene deletion and a hFcRn transgene knock-in (mFcRn$^{-/-}$,+hFcRn) on a C57BL/6J background were used for

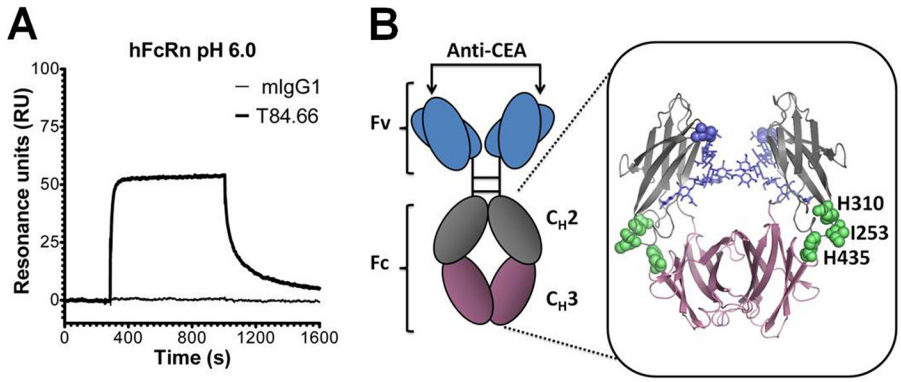

FIGURE 1. **Schematic illustration of the scFv-Fc format and binding of T84.66 to hFcRn.** *A,* representative SPR sensorgrams of anti-hydroxy-5-iodo-3-nitrophenylacetyl mIgG1 and chimeric mouse-human anti-CEA T84.66 IgG1 injected over immobilized hFcRn at pH 6.0. *B,* illustration of the scFv-Fc format. The anti-CEA-binding sites are indicated by *arrows*, and the amino acid residues of the Fc targeted by site-directed mutagenesis (H310A, I253A, H435R, and H435Q) are highlighted as *spheres* (*lime*) in the close-up of the human IgG1-derived Fc crystal structure. The glycans attached to residue Asn-297 within the C_H2 domains are highlighted in *blue*. The C_H2 and C_H3 domains are highlighted in *gray* and *pink*, respectively. The figure was designed using PyMOL with the crystallographic data of the human IgG1 Fc (57). *Fv*, fragment variable; *Fc*, fragment crystallizable; C_H, constant heavy.

these studies (42). Mice were divided into six groups of four mice, each group consisting of two female and two male mice with the exception of the group injected with ^{123}I-labeled scFv-Fc H310A/H435Q that had one female and three male mice. Each animal was injected intravenously with 96–130 μCi of ^{123}I-labeled scFv-Fc proteins (30 μg of labeled protein per mouse) under anesthesia. Immediately after injection (0-h time point), the tip of each mouse tail was nicked with a scalpel, and ~10 μl of blood was collected in a pre-weighed capillary tube. Time points of blood collection were 0, 2, 4, 6, 12, 24, 48, and 72 h. Blood activity was determined using a Wallac WIZARD automatic gamma counter (PerkinElmer Life Sciences Inc.). Results were decay corrected and calculated as percentage of injected dose/g (% ID/g). To calculate the blood clearance times, GraphPad Prism 5 for Windows, Version 5.03 (GraphPad Software Inc.), was used. Two rate constants (k_1 and k_2) characteristic of each engineered fragment were determined. Biexponential functions were fitted to each blood clearance curve (% ID/g) and the distribution ($t_{1/2}\alpha$) and elimination ($t_{1/2}\beta$) half-life of each scFv-Fc molecule in the hFcRn mice was determined.

Statistical Analysis—Significant differences in values were examined by comparing the 95% confidence intervals for the variable estimates. A two-way analysis of variance test (GraphPad Prism 5 for Windows, Version 5.03; GraphPad Software Inc.) was used to compare the following: 1) the blood activity curves of different scFv-Fc proteins in hFcRn mice, and 2) the same scFv-Fc fragment in hFcRn and BALB/c mice (36). Standard error was used to measure variability.

RESULTS

Dramatic Differences in Binding Specificity for mIgG1 and scFv-Fc toward hFcRn and mFcRn—The hFcRn HC shares 66% amino acid sequence identity with the mouse receptor orthologue (supplemental Fig. 1), where several critical key residues involved in the interaction between IgG and FcRn are conserved, such as Glu-115, Glu-116, and Trp-131 localized to the α2-domain (human numbering). However, despite high sequence homology, the human and mouse forms of FcRn show dramatic differences in binding specificity for IgG from a range of animals (20, 22). This finding is confirmed by the SPR analysis where a full-length chimeric mouse-human anti-CEA T84.66 IgG1 consisting of mouse λ light chains and human HCs binds hFcRn reversibly at pH 6.0. In contrast, a fully WT mIgG1, also with λ light chain and with specificity for the hapten hydroxy-5-iodo-3-nitrophenylacetyl, does not bind (Fig. 1*A*).

Regarding the Fc part of the four mouse and human IgG subclasses, a high degree of conservation exists. Amino acid residues central in pH-dependent binding to FcRn are fully conserved, except mIgG2b and hIgG3 that have a Tyr or Arg at position 435, respectively. In addition, distinct differences exist in flanking amino acids that may affect binding (supplemental Fig. 2). The three conserved residues, Ile-253, His-310, and His-435, found at the Fc elbow region were studied in this report, and their location is highlighted in the crystallographic illustration of hIgG1 Fc shown in Fig. 1*B*.

ELISA Measurements of FcRn Binding to the Anti-CEA scFv-Fc Variants—Several anti-CEA scFv-Fc variants have previously been designed based on the monoclonal T84.66 IgG1 (36, 37), schematically illustrated in Fig. 1*B*. Five mutant variants were constructed by site-directed mutagenesis; Ile-253 in the C_H2-domain was mutated to alanine (I253A), His-310 and His-435 within the C_H3 domain were mutated to alanine, glutamine, or arginine (H310A, H435Q, and H435R), respectively. In addition, a double mutant was produced by combining H310A and H435Q (H310A/H435Q). The rationale behind the two mutations of His-435 was to mimic the two protonation states of the histidine residue under acidic (optimal FcRn binding) and neutral pH (no binding or release from the FcRn).

To explore their FcRn binding properties, the mutant variants were initially compared with the WT scFv-Fc counterpart for pH-dependent binding to mFcRn and hFcRn by ELISA. Wells were directly coated with recombinant soluble human CEA followed by capture of titrated amounts of the anti-CEA scFv-Fc variants. The mouse or human forms of GST-tagged FcRn were added, and bound receptors were visualized using an anti-GST-HRP antibody. The experiment was performed at both acidic (pH 6.0) and neutral pH. The WT variant showed

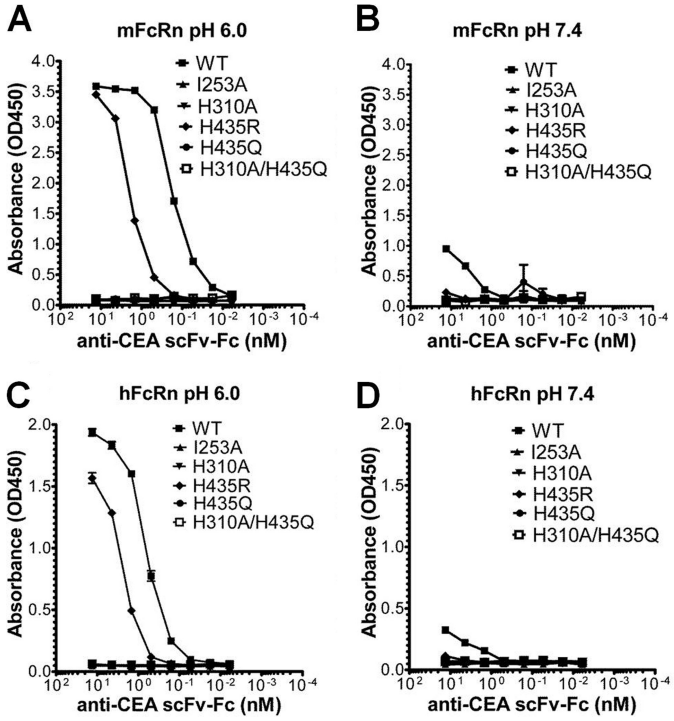

FIGURE 2. **ELISA measurements of pH-dependent binding of mFcRn and hFcRn to the scFv-Fc variants.** Binding responses of mFcRn to titrated amounts of WT, I253A, H310A, H435R, H435Q, and H310A/H435Q at pH 6.0 (*A*) and pH 7.4 (*B*), respectively. Binding of hFcRn to titrated amounts of WT, I253A, H310A, H435R, H435Q, and H310A/H435Q at pH 6.0 (*C*) and pH 7.4 (*D*). The *numbers* given represent the mean of triplicates.

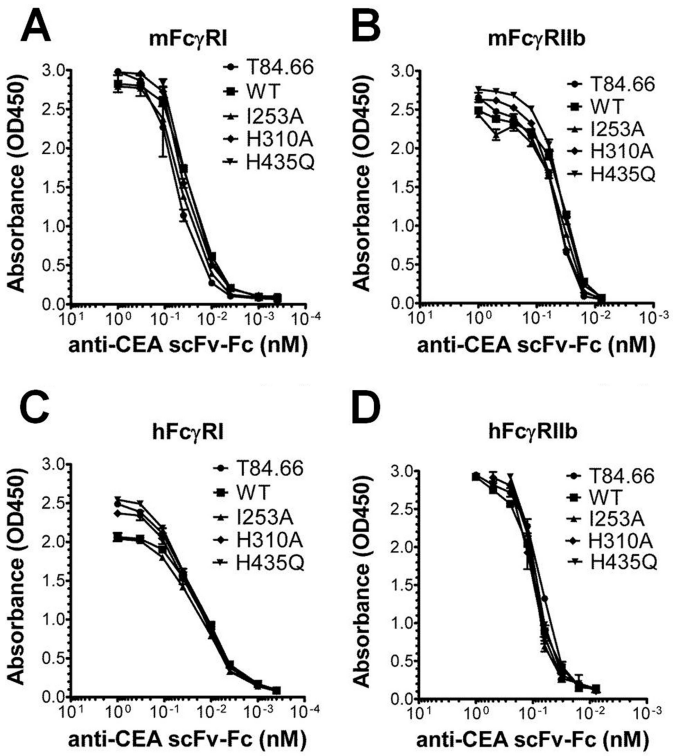

FIGURE 3. **ELISA measurements of FcγR binding to scFv-Fc variants.** Binding of mFcγRI (*A*), mFcγRIIb (*B*), hFcγRI (*C*), and hFcγRIIb (*D*) to titrated amounts of T84.66 and the scFv-Fc variants (WT, I253A, H310A, and H435Q). The *numbers* given represent the mean of triplicates.

pH-dependent binding to both mFcRn and hFcRn (Fig. 2, *A–D*) with considerably stronger binding to mFcRn than hFcRn at acidic pH. The binding responses obtained at neutral pH were very low compared with that at acidic pH, and again, a stronger binding was detected for mFcRn (Fig. 2, *B* and *D*).

The positively charged state of H435R at both acidic and neutral pH might promote FcRn binding at both pH conditions. However, in the ELISA, this molecule showed reduced binding toward both receptor species at pH 6.0, and more so for mFcRn than for hFcRn (Fig. 2, *A* and *C*). At neutral pH, no detectable binding was observed for hFcRn, and the strong binding detected for the WT construct toward mFcRn was lost (Fig. 2, *B* and *D*). The single mutants, I253A and H310A, as well as the double mutant, H310A/H435Q, showed no binding to either receptor (Fig. 2, *A–D*).

Impact of the scFv-Fc Mutant Variants on Binding to the Classical FcγRs—Besides FcRn, the classical FcγRs bind to a nonoverlapping binding site in the lower hinge and C_H2-domain (43). To investigate whether the scFv-Fc format and the introduced mutations had any effect on binding to this class of receptors, we screened T84.66 and some of the scFv-Fc variants for binding to all mouse and human FcγRs using ELISA. The mouse and human high affinity FcγRI and low affinity FcγRIIb were added to titrated amounts of the antibody variants. Only minor binding differences were detected (Fig. 3, *A–D*). Similarly, minor differences in binding capacity were seen for binding to hFcγRIIa, hFcγRIIIa, hFcγRIIIb, mFcγRIII, and mFcγRIV (supplemental Fig. 3).

Differential Binding of the Anti-CEA scFv-Fc Variants to FcRn Revealed by SPR Analysis—The more sensitive SPR assay was employed to complete a detailed characterization of the interaction between the mouse and human forms of FcRn and the anti-CEA scFv-Fc variants. In contrast to ELISA, the SPR technology allows direct visualization of real time macromolecular interactions independent of capture on antigen or "tagging" of the interacting partners using detection antibodies.

In all SPR experiments, soluble forms of FcRn were covalently immobilized on a CM5 biosensor chip to mimic the physiological situation where FcRn is a transmembrane receptor that binds circulating soluble IgG molecules. Initially, we investigated the binding property of the intact anti-CEA T84.66 IgG1 by injected serial dilutions over immobilized mFcRn or hFcRn at pH 6.0. Representative sensorgrams (Fig. 4, *A* and *B*) clearly demonstrate concentration-dependent and reversible binding, although the SPR profiles revealed considerably stronger binding to mFcRn than to the human form. To compare the relative binding properties of the scFv-Fc antibody fragments, samples of 0.5 or 1.0 μM of each variant were injected at pH 6.0 or 7.4 over mFcRn immobilized at two different densities (~110 and ~900 RU). The nonmutated scFv-Fc variant bound strongly to mFcRn at acidic pH, and some binding was also detected at neutral pH (Fig. 5*A*). The same result was obtained for H435R (Fig. 5*D*). Although the binding kinetics at acidic pH were characterized by slow dissociation, interacting molecules dissociated rapidly at neutral pH. All single mutants showed detectable binding to mFcRn at acidic pH, although the

H310A/H435Q double mutant did not. Neither I253A, H310A, H435Q, nor the double mutant bound at neutral pH (Fig. 5, *A–F*). Based on the maximum binding responses obtained at equilibrium (Req) at the two surface densities of immobilized mFcRn at acidic pH (supplemental Table 1), a hierarchy of Req binding responses, ranking from highest to lowest, were as follows: H435R >/ = WT > H435Q > I253A > H310A > H310A/H435Q.

Repeating the SPR assay, using hFcRn immobilized at two different surface densities (~320 and ~1200 RU), overall weaker binding responses than those recorded for binding to mFcRn were obtained at pH 6.0 (Fig. 6, *A–F*). In contrast to the slow dissociation measured for WT scFv-Fc and H435R toward mFcRn, fast dissociation was seen (Fig. 6, *A* and *D*). Furthermore, I253A was the only single point mutant that gave a detectable binding response at acidic pH at the high density surface (Fig. 6*B*). None of the variants bound at neutral pH (Fig. 6, *A–F*). The Req binding responses obtained at both surface densities are listed in supplemental Table 2. Finally, immobilization of a large amount of hFcRn (~4000 RU) also gave rise to detectable binding responses for H310A and H435Q, although no binding was detected for the double mutant (Fig. 6, *G–I*). Thus, a hierarchy of Req binding responses, from highest to lowest, was obtained as follows: H435R > WT > I253A >H435Q > H310A > H310A/H435Q.

To obtain more quantitative binding data, kinetic evaluations were performed by injecting titrated amounts of each of the scFv-Fc variants over the two receptors at pH 6.0. Again, kinetic constants were calculated by fitting the data to the heterogeneous ligand binding model (Table 1).

The WT scFv-Fc fragment showed stronger binding to both mFcRn and hFcRn than the mutants, and all variants bound more strongly to mFcRn than to hFcRn (Table 1). Although the WT bound mFcRn more than 30 times more strongly than hFcRn, the difference was only five times for the H435R mutant. Based on our binding analysis, a hierarchy reflecting strongest to weakest binding to mFcRn and hFcRn appeared as follows: WT > H435R > H435Q > I253A > H310A > H310A/H435Q and WT > H435R > I253A > H435Q > H310A >H310A/H435Q, respectively. Thus, the H435Q mutant bound mFcRn better than I253A, whereas the reverse was the case for the human receptor.

Radiolabeling and Blood Clearance Studies in hFcRn Transgenic Mice—To evaluate the *in vivo* blood clearance rates of the anti-CEA scFv-Fc variants, we used a mouse model with a homozygous mFcRn gene deletion and a hFcRn transgene knock-in (mFcRn$^{-/-}$, +hFcRn) on a C57BL/6J background.

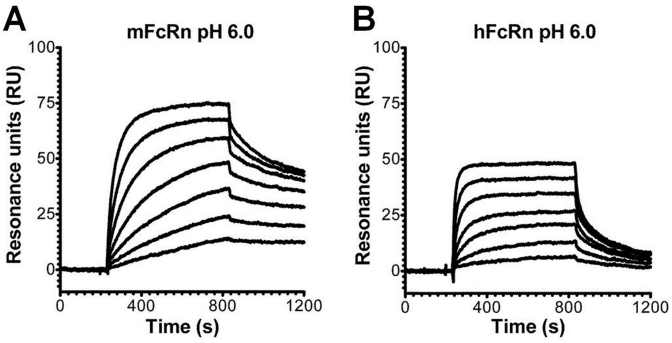

FIGURE 4. **SPR analyses of the interaction of chimeric anti-CEA T84.66 IgG1 with mFcRn and hFcRn.** Representative sensorgrams show serial dilutions of anti-CEA T84.66 IgG1(0.004–1 μM) injected over a flow cell coupled with mFcRn (~300 RU) (*A*) and hFcRn (~400 RU) at a flow rate of 50 μl/min (pH 6.0) (*B*). The sensorgrams were zero-adjusted and reference cell data subtracted.

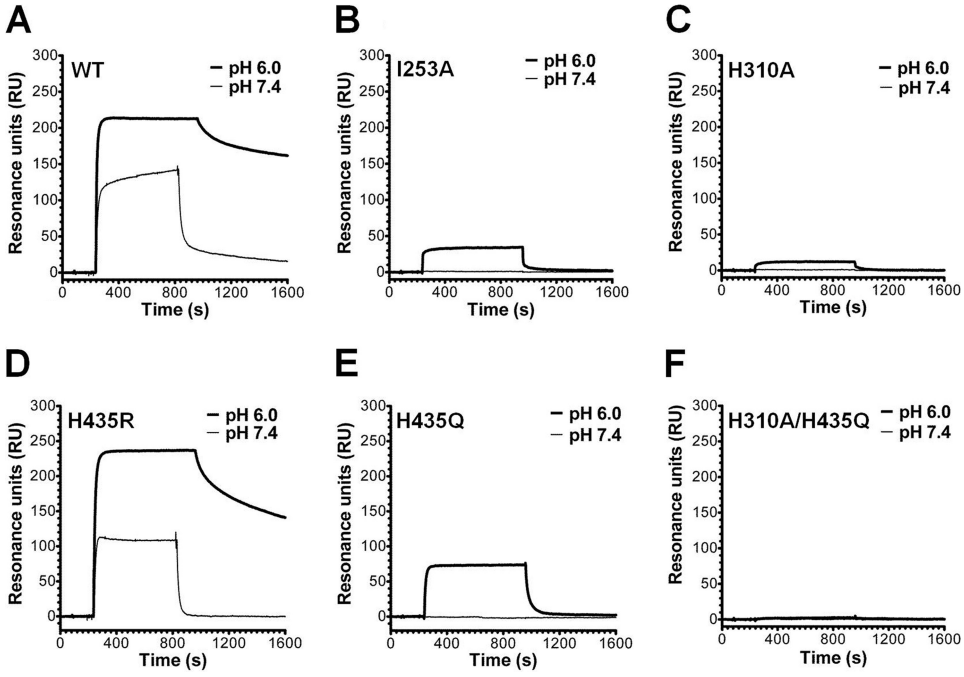

FIGURE 5. **SPR binding profiles of anti-CEA scFv-Fc variants to immobilized mFcRn.** Representative sensorgram overlays obtained with 0.5 μM of the anti-CEA ScFv-Fc variants injected over a flow cell coupled with mFcRn (~900 RU) at a flow rate of 50 μl/min (pH 6.0 and 7.4). *A*, WT; *B*, I253A; *C*, H310A; *D*, H435R; *E*, H435Q; and *F*, H310A/H435Q. The sensorgrams were zero-adjusted and reference cell data subtracted.

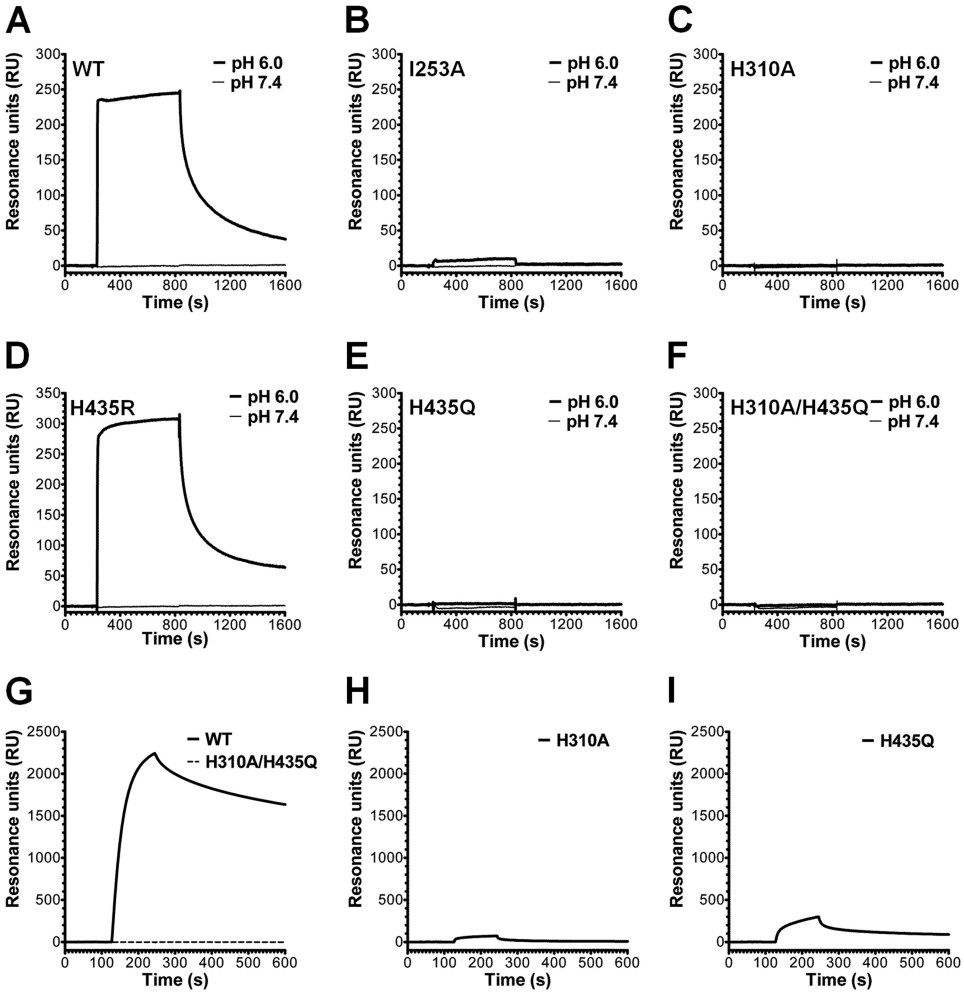

FIGURE 6. **SPR binding profiles of anti-CEA scFv-Fc variants to immobilized hFcRn.** Representative sensorgram overlays obtained with 0.5 μM of each anti-CEA scFv-Fc variant injected over a flow cell coupled with hFcRn (~1200 RU) at a flow rate of 50 μl/min (pH 6.0 and 7.4). *A*, WT; *B*, I253A; *C*, H310A; *D*, H435R; *E*, H435Q; and *F*, H310A/H435Q. Representative sensorgram overlays were obtained with 2.0 μM WT and H310A/H435Q (*G*), H310A (*H*), and H435Q (*I*) and injected over a flow cell coupled with large amounts of hFcRn (~4000 RU) at a flow rate of 50 μl/min (pH 6.0). All sensorgrams were zero-adjusted and reference cell data subtracted.

TABLE 1
SPR-derived affinities of the interaction of scFv-Fc variants with FcRn

scFc-Fc variant	mFcRn K_{D1}	mFcRn K_{D2}	hFcRn K_{D1}	hFcRn K_{D2}
	nM	nM	nM	nM
WT	0.2 ± 0.0	43.8 ± 2.7	6.4 ± 2.6	105.3 ± 64
H435R	1.8 ± 0.1	122.1 ± 55.8	9.4 ± 0.7	196.6 ± 19.3
H435Q	80.9 ± 18.1	400.1 ± 112.8	ND[a]	ND
I253A	443.5 ± 4.9	1054 ± 1.9	ND	ND
H310A	ND	ND	ND	ND
H310A/H435Q	ND	ND	ND	ND

[a] ND mean not determined because of no binding or very weak binding.

The scFv-Fc variants were radiolabeled, and the efficiency for the ^{123}I radiolabeling reaction averaged 82.9%, ranging from 69.7% (WT) to 88.4% (I253A), although the mean specific activity was 2.59 ± 0.131 μCi/μg, ranging from 2.23 to 3.12 μCi/μg. The blood activity data at 0.5, 2, 4, 6, 12, 24, 48, and 72 h post-injection were measured. Analysis of variance between the blood activity curves (Fig. 7) was done using analysis of variance and revealed that all six scFv-Fc fragments had significantly different blood clearance profile with p values ranging from < 0.0001 to 0.049. The rate constants (k_1 and k_2), the area under the curve derived from the fitted curves, and the calculated distribution ($t_{½}\alpha$) and elimination ($t_{½}\beta$) half-lives of each scFv-Fc protein in blood are summarized in Table 2. The order of blood clearance based on the area under the curve, from slow to fast, is as follows: WT > H435R > I253A > H435Q > H310A/H435Q > H310A.

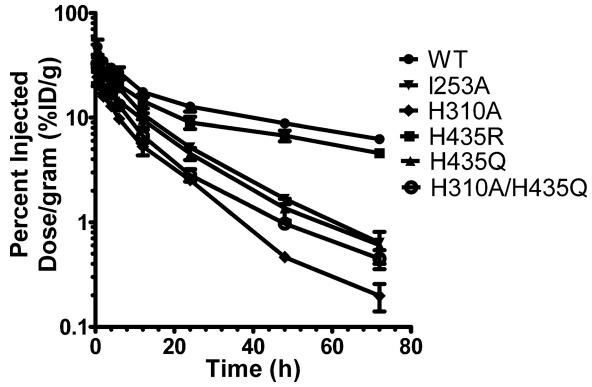

FIGURE 7. **Blood activity curves of ^{123}I-labeled scFv-Fc fragments in hFcRn transgenic mice.** Mice were injected with 96–130 μCi of ^{123}I-labeled scFv-Fc proteins (30 μg of labeled protein/mouse) under anesthesia. Blood samples were collected from the tail immediately after injection (0-h time point) and at time points 2, 4, 6, 12, 24, 48, and 72 h post-injection. Blood activity was determined using a Wallac WIZARD automatic gamma. The percentage of injected dose/g (*% ID/g*) was calculated. Each group represents four mice. Logarithmic scale, S.E. was used to measure variability.

Blood Clearance in BALB/c (mFcRn) Versus hFcRn Transgenic Mice—The same scFv-Fc proteins used in this work have previously been radioiodinated and evaluated for their blood clearance rates in WT BALB/c mice (36). When comparing the two sets of blood elimination curves, each scFv-Fc protein exhibited considerably faster elimination from the blood in hFcRn mice than in WT BALB/c mice (Fig. 8, *A*–*F*). The most striking difference, however, is the change in the order of clearance. In WT BALB/c, the blood clearance order, from slow to fast, was as follows: scFv-Fc WT > H435R > H435Q > I253A > H310A > H310A/H435Q. Furthermore, the H435R mutant cleared much faster than scFv-Fc WT in WT BALB/c mice, whereas the difference between the two was very small in hFcRn mice. Statistical comparison of the blood activity curves of the same scFv-Fc fragment in BALB/c and hFcRn transgenic mice showed that all pairs of blood clearance curves are statistically different (p value ranging from <0.0001 to 0.0068), except for the scFv-Fc H310A/H435Q double mutant (p = 0.051) that behaves the same in mice expressing mouse or human FcRn (supplemental Table 3).

TABLE 2
Blood half-lives of ^{123}I-labeled T84.66 scFv-Fc antibody fragments in hFcRn mice

Antibody fragment	Aα[a]	Aβ[a]	k_1[b]	k_2[b]	$t_{1/2}$[c]	$t_{1/2}$[c]	AUC[d]
	%ID/g	*%ID/g*	*1/h*	*1/h*	*h*	*h*	
Wild type	29.6	20.3	0.2497	0.01737	2.776	39.89	938.3
H435R	22.6	14.4	0.2042	0.0165	3.394	42.02	710.6
H435Q	21.2	22.2	1.244	0.06761	0.5573	10.25	361.6
I253A	8.7	28.6	0.9073	0.07431	0.764	9.328	427.1
H310A	13.2	17.6	1.108	0.09282	0.6258	7.468	217.3
H310A/H435Q	52.8	26.1	3.766	0.1083	0.1841	6.401	288.2

[a] Amplitudes of the two components are given by Aα and Aβ, where the sum of Aα and Aβ is the total injected dose/g (%ID/g).
[b] k_1 and k_2 are first-order rate constants for distribution and elimination, respectively.
[c] $t_{1/2}\alpha$ and $t_{1/2}\beta$ are the distribution and elimination phase half-lives and are calculated by ln2/k_1 and ln2/k_2, respectively.
[d] Area under the curve is a time integral of the blood uptake (%ID/g·h).

DISCUSSION

In this report, we studied the effect of mutations in the Fc elbow region of chimeric anti-CEA T84.66 scFv-Fc variants on pH-dependent binding to the mouse and human forms of FcRn. Three amino acids, found to be highly conserved and situated in the core binding site for FcRn (Ile-253, His-310, and His-435; highlighted in Fig. 1*B*), were targeted. Although ELISA detected receptor binding to the WT and H435R mutant, the more sensitive method SPR detected a hierarchy of binding responses to both mFcRn and hFcRn. All mutant molecules had none or reduced binding activity compared with WT scFv-Fc.

Introduction of such point mutations in the Fc of IgG or Fc fragment fusions have previously been reported to result in reduced binding to FcRn and correspondingly shorter half-lives or reduced transcellular transport (17, 18, 44–46). However, no study has reported a systematic evaluation of the FcRn binding activity of a matched set of scFv-Fc variants toward FcRn from both mouse and man and correlated the results with serum half-life in WT mice as well as mice expressing only the human form of the receptor. We found that the set of six anti-CEA scFv-Fc variants showed an order of binding to mFcRn (WT > H435R > H435Q > I253A > H310A > H310A/H435Q) that correlated with previously obtained serum half-lives from blood clearance studies in WT BALB/c mice (36).

Binding of the scFv-Fc variants to hFcRn revealed that the affinities were considerably lower than those measured for binding to mFcRn. Although hFcRn interacted strongly with WT and H435R, only weak binding to I253A, H310A, and H435Q was observed, and H310A/H435Q did not bind at all.

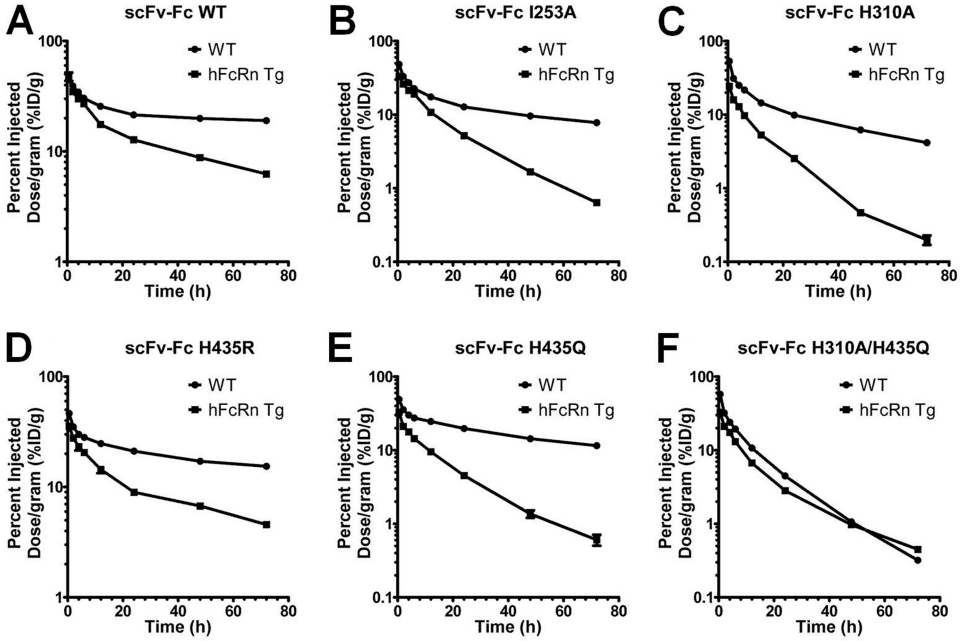

FIGURE 8. **Blood clearance curves of ^{123}I-labeled scFv-Fc variants in WT BALB/c mice and hFcRn transgenic mice.** Blood samples were collected from the tail immediately after injection (0-h time point) and at time points 2, 4, 6, 12, 24, 48, and 72 h post-injection. Blood activity was determined using a Wallac WIZARD automatic gamma. The percentage of injected dose per gram (*% ID/g*) was calculated. Each group represents four mice. Logarithmic scale, S.E. was used to measure variability.

The H435R mutant showed slightly higher Req binding responses for both mFcRn and hFcRn compared with the WT, although K_{D1} was lower for the WT. Another difference was that H435Q bound more strongly than I253A to the mouse receptor, whereas I253A bound more strongly to shFcRn than H435Q. Thus, differences in the order of binding of the scFv-Fc mutants to the two receptor species were detected.

Mice are not necessarily ideal models from which half-life in humans may be predicted. Major differences in binding of hIgG1 variants to FcRn from mouse and man have already been demonstrated (20, 21, 25, 28), and the phenomenon clearly underscores the importance of considering cross-species FcRn binding properties of engineered IgG variants and Fc fusion molecules. Rather, direct measurement of the binding affinity of novel engineered IgG variants toward both hFcRn and the FcRn species used for *in vivo* evaluations should be tested.

In this report, we evaluated the blood clearance activity in a mouse strain that lacks expression of its endogenous FcRn HC and is transgenic for the hFcRn HC (42). The rate of blood clearance correlated with binding to recombinant soluble hFcRn, and low binding corresponded to fast clearance. The hierarchy of binding from high to low corresponded to the clearance rates from slow to fast. However, the order of clearance differed from that obtained in WT mice. Thus, the order of clearance depends on the FcRn variant expressed by the mice used.

The histidine residues situated at the Fc elbow are key players in the interaction with FcRn. The H435R and H435Q mutants were generated to mimic the two protonation states of the His-435 residue during the transition from the physiological pH of the bloodstream to the acidic environment in endosomal compartments. At neutral pH, the histidine imidazole side chain is uncharged, although at acidic pH it is positive. Arginine is positively charged at either pH, whereas glutamine is neutral.

Both the H435R and H435Q mutations had an impact on FcRn binding, where H435R showed a somewhat reduced but still considerable binding at acidic pH, compared with H435Q that only interacted weakly with the receptors. The H435R mutant did not show stronger binding at physiological pH, where H435Q did not bind. These results are in agreement with a shorter half-life in WT BALB/c mice where H435R showed a 3.5-fold drop in half-life followed by H435Q (5.5-fold) (36).

The biodistribution data obtained from WT mouse studies are informative to understand how a single amino acid Fc substitution affects half-life in mice. Interestingly, the dramatic effect on clearance of H435R in WT mice may reflect the difference in serum half-life observed between hIgG1 (His-435) and hIgG3 (Arg-435) in humans, where hIgG1 has a three times longer half-life than hIgG3 (21 *versus* 7 days) (47–49). We recently reported that the short half-life of hIgG3 is due to preferential binding of hIgG1 to FcRn, which is present in a 10-fold higher concentration than hIgG3 in blood. The effect was reversed when Arg-435 of hIgG3 was replaced with a histidine (R435H), and the His-435 of IgG1 was replaced with an arginine (50). In contrast, the *in vivo* data presented here from hFcRn transgenic mice, show only minor differences in blood clearance between H435R and the WT. This may well be due to the fact that these mice have very low endogenous IgG serum levels, as endogenous IgG binds hFcRn very poorly (20, 22).

The hydrophobic Ile-253 is located centrally at the interaction interface and is important for proper packing of the complex (51). Its importance is reflected in the great effect on half-life when mutated to alanine, as shown in this study, where the I253A variant showed a 5.5- and 4.3-fold decreased half-life in WT and hFcRn transgenic mice, respectively (36). The H310A mutant interacted only weakly with FcRn from both species, as mirrored by its short half-life in both mouse strains. Furthermore, the importance of the conserved His-310 and His-435 was also demonstrated for the double mutant (H310A/H435Q), which cleared most rapidly from the blood circulation, as expected.

Several of the scFv-Fc mutants have been evaluated in different mouse tumor models. Initially, the fastest clearing double mutant was shown to be optimal for imaging in CEA-positive LS174T xenografted athymic mice examined by positron emission tomography, followed by H310A, although the I253A, H435Q, H435R, and WT variants were eliminated at much slower rates and thus gave poor tissue to tumor ratios (36, 37). Furthermore, anti-CEA scFv-Fc H310A has been shown to be an attractive candidate for targeting of pancreatic cancer in CEA-positive pancreas cancer xenografted mice (52). In addition, the double mutant with specificity for either human epidermal growth factor receptor 2 (HER2) or CD20 has demonstrated favorable positron emission tomography imaging in nude mice with MCF7/HER2 breast cancer or mice carrying human CD20 expressing lymphomas, respectively (53, 54).

H310A/H435Q degraded in the liver of both tumor-free and mice xenografted with CEA-positive tumor much faster than the single mutant I253A (supplemental Fig. 4) (37). In this study, radiometal labeling of the scFv-Fc variants via a bifunctional chelator was used, as this conjugation is more stable *in vivo* than radioiodination (55). Thus, liver accumulation of radiometal-labeled scFv-Fc mutants correlated with the rate of blood clearance (37).

FcRn has been shown to be expressed in the mouse liver (9), and we have detected FcRn in human hepatocyte cell lines and liver tissue biopsies[7] These findings indicate that FcRn expressed by the liver may function to rescue endogenous IgG and injected radioconjugated IgG Fc fragments with retained FcRn binding activity from intracellular degradation, although noninteracting mutants accumulate and degrade. This mechanism should be considered in further studies as liver accumulation and toxicity may become dose-limiting in antibody-based radiometal therapy. Hence, our findings suggest that IgG or Fc fragments such as the scFv-Fc mutants with substantially reduced FcRn binding capacity may be trapped within this vital organ, although single mutants such as I253A and H310A may be better choices for radioimmunotherapy because of lower liver accumulation and potential toxicity.

Regarding expanding these studies to a more humanized *in vivo* system, immunodeficient mice ($Rag1^{-/-}$) transgenic for hFcRn have recently been described (56). Such mice may be

[7] M. B. Daba, J. T. Andersen, and I. Sandlie, unpublished data.

more ideal in the next phase of *in vivo* evaluations of tumor targeting and imaging using the Fc-engineered scFv-Fc variants.

Acknowledgments—We are grateful to Sathiaruby Sivaganesh for excellent technical assistance. We thank Dr. Derek W. Bartlett (Imaginab Inc., Los Angeles) for assistance with pharmacokinetic analysis.

REFERENCES

1. Holliger, P., and Hudson, P. J. (2005) Engineered antibody fragments and the rise of single domains. *Nat. Biotechnol.* **23,** 1126–1136
2. Kenanova, V., and Wu, A. M. (2006) Tailoring antibodies for radionuclide delivery. *Expert Opin. Drug Deliv.* **3,** 53–70
3. Wu, A. M., and Senter, P. D. (2005) Arming antibodies. Prospects and challenges for immunoconjugates. *Nat. Biotechnol.* **23,** 1137–1146
4. Ghetie, V., Popov, S., Borvak, J., Radu, C., Matesoi, D., Medesan, C., Ober, R. J., and Ward, E. S. (1997) Increasing the serum persistence of an IgG fragment by random mutagenesis. *Nat. Biotechnol.* **15,** 637–640
5. Kamei, D. T., Lao, B. J., Ricci, M. S., Deshpande, R., Xu, H., Tidor, B., and Lauffenburger, D. A. (2005) Quantitative methods for developing Fc mutants with extended half-lives. *Biotechnol. Bioeng.* **92,** 748–760
6. Roopenian, D. C., Christianson, G. J., Sproule, T. J., Brown, A. C., Akilesh, S., Jung, N., Petkova, S., Avanessian, L., Choi, E. Y., Shaffer, D. J., Eden, P. A., and Anderson, C. L. (2003) The MHC class I-like IgG receptor controls perinatal IgG transport, IgG homeostasis, and fate of IgG-Fc-coupled drugs. *J. Immunol.* **170,** 3528–3533
7. Akilesh, S., Huber, T. B., Wu, H., Wang, G., Hartleben, B., Kopp, J. B., Miner, J. H., Roopenian, D. C., Unanue, E. R., and Shaw, A. S. (2008) Podocytes use FcRn to clear IgG from the glomerular basement membrane. *Proc. Natl. Acad. Sci. U.S.A.* **105,** 967–972
8. Blumberg, R. S., Koss, T., Story, C. M., Barisani, D., Polischuk, J., Lipin, A., Pablo, L., Green, R., and Simister, N. E. (1995) A major histocompatibility complex class I-related Fc receptor for IgG on rat hepatocytes. *J. Clin. Invest.* **95,** 2397–2402
9. Akilesh, S., Christianson, G. J., Roopenian, D. C., and Shaw, A. S. (2007) Neonatal FcR expression in bone marrow-derived cells functions to protect serum IgG from catabolism. *J. Immunol.* **179,** 4580–4588
10. Zhu, X., Meng, G., Dickinson, B. L., Li, X., Mizoguchi, E., Miao, L., Wang, Y., Robert, C., Wu, B., Smith, P. D., Lencer, W. I., and Blumberg, R. S. (2001) MHC class I-related neonatal Fc receptor for IgG is functionally expressed in monocytes, intestinal macrophages, and dendritic cells. *J. Immunol.* **166,** 3266–3276
11. Qiao, S. W., Kobayashi, K., Johansen, F. E., Sollid, L. M., Andersen, J. T., Milford, E., Roopenian, D. C., Lencer, W. I., and Blumberg, R. S. (2008) Dependence of antibody-mediated presentation of antigen on FcRn. *Proc. Natl. Acad. Sci. U.S.A.* **105,** 9337–9342
12. Baker, K., Qiao, S. W., Kuo, T. T., Aveson, V. G., Platzer, B., Andersen, J. T., Sandlie, I., Chen, Z., de Haar, C., Lencer, W. I., Fiebiger, E., and Blumberg, R. S. (2011) Neonatal Fc receptor for IgG (FcRn) regulates cross-presentation of IgG immune complexes by CD8-CD11b$^+$ dendritic cells. *Proc. Natl. Acad. Sci. U.S.A.* **108,** 9927–9932
13. Montoyo, H. P., Vaccaro, C., Hafner, M., Ober, R. J., Mueller, W., and Ward, E. S. (2009) Conditional deletion of the MHC class I-related receptor FcRn reveals the sites of IgG homeostasis in mice. *Proc. Natl. Acad. Sci. U.S.A.* **106,** 2788–2793
14. Ward, E. S., Zhou, J., Ghetie, V., and Ober, R. J. (2003) Evidence to support the cellular mechanism involved in serum IgG homeostasis in humans. *Int. Immunol.* **15,** 187–195
15. Ober, R. J., Martinez, C., Lai, X., Zhou, J., and Ward, E. S. (2004) Exocytosis of IgG as mediated by the receptor, FcRn. An analysis at the single-molecule level. *Proc. Natl. Acad. Sci. U.S.A.* **101,** 11076–11081
16. Prabhat, P., Gan, Z., Chao, J., Ram, S., Vaccaro, C., Gibbons, S., Ober, R. J., and Ward, E. S. (2007) Elucidation of intracellular recycling pathways leading to exocytosis of the Fc receptor, FcRn, by using multifocal plane microscopy. *Proc. Natl. Acad. Sci. U.S.A.* **104,** 5889–5894
17. Kim, J. K., Firan, M., Radu, C. G., Kim, C. H., Ghetie, V., and Ward, E. S. (1999) Mapping the site on human IgG for binding of the MHC class I-related receptor, FcRn. *Eur. J. Immunol.* **29,** 2819–2825
18. Medesan, C., Matesoi, D., Radu, C., Ghetie, V., and Ward, E. S. (1997) Delineation of the amino acid residues involved in transcytosis and catabolism of mouse IgG1. *J. Immunol.* **158,** 2211–2217
19. Raghavan, M., Chen, M. Y., Gastinel, L. N., and Bjorkman, P. J. (1994) Investigation of the interaction between the class I MHC-related Fc receptor and its immunoglobulin G ligand. *Immunity* **1,** 303–315
20. Ober, R. J., Radu, C. G., Ghetie, V., and Ward, E. S. (2001) Differences in promiscuity for antibody-FcRn interactions across species. Implications for therapeutic antibodies. *Int. Immunol.* **13,** 1551–1559
21. Zhou, J., Mateos, F., Ober, R. J., and Ward, E. S. (2005) Conferring the binding properties of the mouse MHC class I-related receptor, FcRn, onto the human ortholog by sequential rounds of site-directed mutagenesis. *J. Mol. Biol.* **345,** 1071–1081
22. Andersen, J. T., Daba, M. B., Berntzen, G., Michaelsen, T. E., and Sandlie, I. (2010) Cross-species binding analyses of mouse and human neonatal Fc receptor show dramatic differences in immunoglobulin G and albumin binding. *J. Biol. Chem.* **285,** 4826–4836
23. Hinton, P. R., Johlfs, M. G., Xiong, J. M., Hanestad, K., Ong, K. C., Bullock, C., Keller, S., Tang, M. T., Tso, J. Y., Vásquez, M., and Tsurushita, N. (2004) Engineered human IgG antibodies with longer serum half-lives in primates. *J. Biol. Chem.* **279,** 6213–6216
24. Hinton, P. R., Xiong, J. M., Johlfs, M. G., Tang, M. T., Keller, S., and Tsurushita, N. (2006) An engineered human IgG1 antibody with longer serum half-life. *J. Immunol.* **176,** 346–356
25. Petkova, S. B., Akilesh, S., Sproule, T. J., Christianson, G. J., Al Khabbaz, H., Brown, A. C., Presta, L. G., Meng, Y. G., and Roopenian, D. C. (2006) Enhanced half-life of genetically engineered human IgG1 antibodies in a humanized FcRn mouse model. Potential application in humorally mediated autoimmune disease. *Int. Immunol.* **18,** 1759–1769
26. Dall'Acqua, W. F., Kiener, P. A., and Wu, H. (2006) Properties of human IgG1s engineered for enhanced binding to the neonatal Fc receptor (FcRn). *J. Biol. Chem.* **281,** 23514–23524
27. Blumberg, R. S., and Lencer, W. I. (2005) Antibodies in the breakdown lane. *Nat. Biotechnol.* **23,** 1232–1234
28. Vaccaro, C., Zhou, J., Ober, R. J., and Ward, E. S. (2005) Engineering the Fc region of immunoglobulin G to modulate *in vivo* antibody levels. *Nat. Biotechnol.* **23,** 1283–1288
29. Vaccaro, C., Bawdon, R., Wanjie, S., Ober, R. J., and Ward, E. S. (2006) Divergent activities of an engineered antibody in murine and human systems have implications for therapeutic antibodies. *Proc. Natl. Acad. Sci. U.S.A.* **103,** 18709–18714
30. Wu, A. M., Yazaki, P. J., Tsai, S., Nguyen, K., Anderson, A. L., McCarthy, D. W., Welch, M. J., Shively, J. E., Williams, L. E., Raubitschek, A. A., Wong, J. Y., Toyokuni, T., Phelps, M. E., and Gambhir, S. S. (2000) High resolution microPET imaging of carcinoembryonic antigen-positive xenografts by using a copper-64-labeled engineered antibody fragment. *Proc. Natl. Acad. Sci. U.S.A.* **97,** 8495–8500
31. Sundaresan, G., Yazaki, P. J., Shively, J. E., Finn, R. D., Larson, S. M., Raubitschek, A. A., Williams, L. E., Chatziioannou, A. F., Gambhir, S. S., and Wu, A. M. (2003) ^{124}I-Labeled engineered anti-CEA minibodies and diabodies allow high contrast, antigen-specific small animal PET imaging of xenografts in athymic mice. *J. Nucl. Med.* **44,** 1962–1969
32. Wong, J. Y., Chu, D. Z., Williams, L. E., Yamauchi, D. M., Ikle, D. N., Kwok, C. S., Liu, A., Wilczynski, S., Colcher, D., Yazaki, P. J., Shively, J. E., Wu, A. M., and Raubitschek, A. A. (2004) Pilot trial evaluating a ^{123}I-labeled 80-kilodalton engineered anticarcinoembryonic antigen antibody fragment (cT84.66 minibody) in patients with colorectal cancer. *Clin. Cancer Res.* **10,** 5014–5021
33. Hu, S., Shively, L., Raubitschek, A., Sherman, M., Williams, L. E., Wong, J. Y., Shively, J. E., and Wu, A. M. (1996) Minibody. A novel engineered anti-carcinoembryonic antigen antibody fragment (single-chain Fv-CH3) that exhibits rapid, high level targeting of xenografts. *Cancer Res.* **56,** 3055–3061
34. Boucher, D., Cournoyer, D., Stanners, C. P., and Fuks, A. (1989) Studies on the control of gene expression of the carcinoembryonic antigen family in human tissue. *Cancer Res.* **49,** 847–852

35. Esteban, J. M., Paxton, R., Mehta, P., Battifora, H., and Shively, J. E. (1993) Sensitivity and specificity of Gold types 1–5 anti-carcinoembryonic antigen monoclonal antibodies. Immunohistologic characterization in colorectal cancer and normal tissues. *Hum. Pathol.* **24,** 322–328
36. Kenanova, V., Olafsen, T., Crow, D. M., Sundaresan, G., Subbarayan, M., Carter, N. H., Ikle, D. N., Yazaki, P. J., Chatziioannou, A. F., Gambhir, S. S., Williams, L. E., Shively, J. E., Colcher, D., Raubitschek, A. A., and Wu, A. M. (2005) Tailoring the pharmacokinetics and positron emission tomography imaging properties of anti-carcinoembryonic antigen single-chain Fv-Fc antibody fragments. *Cancer Res.* **65,** 622–631
37. Kenanova, V., Olafsen, T., Williams, L. E., Ruel, N. H., Longmate, J., Yazaki, P. J., Shively, J. E., Colcher, D., Raubitschek, A. A., and Wu, A. M. (2007) Radioiodinated *versus* radiometal-labeled anti-carcinoembryonic antigen single-chain Fv-Fc antibody fragments. Optimal pharmacokinetics for therapy. *Cancer Res.* **67,** 718–726
38. Andersen, J. T., Justesen, S., Fleckenstein, B., Michaelsen, T. E., Berntzen, G., Kenanova, V. E., Daba, M. B., Lauvrak, V., Buus, S., and Sandlie, I. (2008) Ligand binding and antigenic properties of a human neonatal Fc receptor with mutation of two unpaired cysteine residues. *FEBS J.* **275,** 4097–4110
39. Popov, S., Hubbard, J. G., Kim, J., Ober, B., Ghetie, V., and Ward, E. S. (1996) The stoichiometry and affinity of the interaction of murine Fc fragments with the MHC class I-related receptor, FcRn. *Mol. Immunol.* **33,** 521–530
40. Berntzen, G., Lunde, E., Flobakk, M., Andersen, J. T., Lauvrak, V., and Sandlie, I. (2005) Prolonged and increased expression of soluble Fc receptors, IgG and a TCR-Ig fusion protein by transiently transfected adherent 293E cells. *J. Immunol. Methods* **298,** 93–104
41. Blumberg, D., Hochwald, S., Brennan, M. F., and Burt, M. (1995) Interleukin-6 stimulates gluconeogenesis in primary cultures of rat hepatocytes. *Metabolism* **44,** 145–146
42. Stein, C., Kling, L., Proetzel, G., Roopenian, D. C., de Angelis, M. H., Wolf, E., and Rathkolb, B. (2012) Clinical chemistry of human FcRn transgenic mice. *Mamm. Genome* **23,** 259–269
43. Nimmerjahn, F., and Ravetch, J. V. (2008) Fcγ receptors as regulators of immune responses. *Nat. Rev. Immunol.* **8,** 34–47
44. Firan, M., Bawdon, R., Radu, C., Ober, R. J., Eaken, D., Antohe, F., Ghetie, V., and Ward, E. S. (2001) The MHC class I-related receptor, FcRn, plays an essential role in the maternofetal transfer of γ-globulin in humans. *Int. Immunol.* **13,** 993–1002
45. Bitonti, A. J., Dumont, J. A., Low, S. C., Peters, R. T., Kropp, K. E., Palombella, V. J., Stattel, J. M., Lu, Y., Tan, C. A., Song, J. J., Garcia, A. M., Simister, N. E., Spiekermann, G. M., Lencer, W. I., and Blumberg, R. S. (2004) Pulmonary delivery of an erythropoietin Fc fusion protein in non-human primates through an immunoglobulin transport pathway. *Proc. Natl. Acad. Sci. U.S.A.* **101,** 9763–9768
46. Spiekermann, G. M., Finn, P. W., Ward, E. S., Dumont, J., Dickinson, B. L., Blumberg, R. S., and Lencer, W. I. (2002) Receptor-mediated immunoglobulin G transport across mucosal barriers in adult life: functional expression of FcRn in the mammalian lung. *J. Exp. Med.* **196,** 303–310
47. Spiegelberg, H. L., Fishkin, B. G., and Grey, H. M. (1968) Catabolism of human γG-immunoglobulins of different heavy chain subclasses. I. Catabolism of γG-myeloma proteins in man. *J. Clin. Invest.* **47,** 2323–2330
48. Morell, A., Terry, W. D., and Waldmann, T. A. (1970) Metabolic properties of IgG subclasses in man. *J. Clin. Invest.* **49,** 673–680
49. Spiegelberg, H. L. (1974) Biological activities of immunoglobulins of different classes and subclasses. *Adv. Immunol.* **19,** 259–294
50. Stapleton, N. M., Andersen, J. T., Stemerding, A. M., Bjarnarson, S. P., Verheul, R. C., Gerritsen, J., Zhao, Y., Kleijer, M., Sandlie, I., de Haas, M., Jonsdottir, I., van der Schoot, C. E., and Vidarsson, G. (2011) Competition for FcRn-mediated transport gives rise to short half-life of human IgG3 and offers therapeutic potential. *Nat. Commun.* **2,** 599
51. Martin, W. L., West, A. P., Jr., Gan, L., and Bjorkman, P. J. (2001) Crystal structure at 2.8 Å of an FcRn/heterodimeric Fc complex. Mechanism of pH-dependent binding. *Mol. Cell* **7,** 867–877
52. Girgis, M. D., Olafsen, T., Kenanova, V., McCabe, K. E., Wu, A. M., and Tomlinson, J. S. (2011) Targeting CEA in pancreas cancer xenografts with a mutated scFv-Fc antibody fragment. *EJNMMI Res.* **1,** 24
53. Olafsen, T., Kenanova, V. E., Sundaresan, G., Anderson, A. L., Crow, D., Yazaki, P. J., Li, L., Press, M. F., Gambhir, S. S., Williams, L. E., Wong, J. Y., Raubitschek, A. A., Shively, J. E., and Wu, A. M. (2005) Optimizing radiolabeled engineered anti-p185HER2 antibody fragments for *in vivo* imaging. *Cancer Res.* **65,** 5907–5916
54. Olafsen, T., Sirk, S. J., Betting, D. J., Kenanova, V. E., Bauer, K. B., Ladno, W., Raubitschek, A. A., Timmerman, J. M., and Wu, A. M. (2010) ImmunoPET imaging of B-cell lymphoma using ^{124}I-anti-CD20 scFv dimers (diabodies). *Protein Eng. Des. Sel.* **23,** 243–249
55. Milenic, D. E., Brady, E. D., and Brechbiel, M. W. (2004) Antibody-targeted radiation cancer therapy. *Nat. Rev. Drug Discov.* **3,** 488–499
56. Zalevsky, J., Chamberlain, A. K., Horton, H. M., Karki, S., Leung, I. W., Sproule, T. J., Lazar, G. A., Roopenian, D. C., and Desjarlais, J. R. (2010) Enhanced antibody half-life improves *in vivo* activity. *Nat. Biotechnol.* **28,** 157–159
57. Deisenhofer, J. (1981) Crystallographic refinement and atomic models of a human Fc fragment and its complex with fragment B of protein A from *Staphylococcus aureus* at 2.9- and 2.8-Å resolution. *Biochemistry* **20,** 2361–2370